Title

Investigating polypropylene-poly(ethylene oxide)-polypropylene triblock copolymers as solid polymer electrolytes for lithium batteries

Authors

Young, Nicholas P
Devaux, Didier
Khurana, Rachna
et al.

Publication Date

2014-10-01

DOI

10.1016/j.ssi.2014.05.012

Peer reviewed

Solid State Ionics 263 (2014) 87–94

Contents lists available at ScienceDirect

Solid State Ionics

journal homepage: www.elsevier.com/locate/ssi

Investigating polypropylene-poly(ethylene oxide)-polypropylene triblock copolymers as solid polymer electrolytes for lithium batteries ☆

Nicholas P. Young [a], Didier Devaux [b], Rachna Khurana [c], Geoffrey W. Coates [c,*], Nitash P. Balsara [a,b,d,**]

[a] Department of Chemical and Biomolecular Engineering, University of California, Berkeley, CA 94720, USA
[b] Environmental Energy Technologies Division, Lawrence Berkeley National Laboratory, Berkeley, CA 94720, USA
[c] Department of Chemistry and Chemical Biology, Baker Laboratory, Cornell University, Ithaca, NY 14853, USA
[d] Materials Sciences Division, Lawrence Berkeley National Laboratory, Berkeley, CA 94720, USA

ARTICLE INFO

Article history:
Received 24 February 2014
Received in revised form 15 May 2014
Accepted 19 May 2014
Available online 7 June 2014

Keywords:
Triblock copolymer
Syndiotactic polypropylene
Poly(ethylene oxide)
Solid polymer electrolyte

ABSTRACT

Syndiotactic polypropylene-*b*-poly(ethylene oxide)-*b*-syndiotactic polypropylene (PEOP) triblock copolymers were synthesized and solid polymer electrolytes were prepared by mixing with lithium bis(trifluoromethane) sulfonimide (LiTFSI) salt. PEOP formed strongly-segregated morphologies in the absence and presence of LiTFSI. LiTFSI inhibited poly(ethylene oxide) crystallization without affecting polypropylene crystallinity. The conductivity exhibited a non-monotonic dependence on molecular weight (M_n) with a maximum near 20 kg/mol. In contrast, polystyrene-*b*-poly(ethylene oxide) electrolytes exhibit conductivity increasing monotonically with M_n, up to a plateau in the high-M_n limit. This suggests that non-conducting semi-crystalline microphases interfere with conducting pathways, while non-conducting amorphous microphases formed well-connected conducting pathways.

Published by Elsevier B.V.

1. Introduction

It is believed that solid polymer electrolytes (SPEs) are essential for the development of next-generation high performance rechargeable batteries comprising a lithium metal anode [1–4]. Extensive work has shown that poly(ethylene oxide) (PEO) possesses good ionic conductivity when doped with alkali metal salts [5]. Subsequent implementation of PEO in full cell experiments has demonstrated its potential for use as a practical SPE [6–8]. In salt-containing PEO, ionic transport is linked to segmental motion [9,10], and transport occurs predominantly in the amorphous phase [11,12]. Thus SPE-based batteries must be operated at temperatures (T) above the PEO melting temperature, $T_{m,PEO}$. However it has been shown that the mechanical properties of PEO in the amorphous phase are insufficient to prevent short circuit due to lithium dendrite growth originating at the lithium metal anode during battery cycling [13,14]. The design of a SPE material which pairs high ionic conductivity with robust mechanical properties is thus an area of significant interest.

In light of the challenges associated with creating an optimal SPE, a variety of polymeric systems have been investigated. Molecular architectures such as comb-like copolymers [15,16], cross-linked polymer networks [17,18], graft copolymers [19–22], and block copolymers [19,23] have been investigated for use as electrolytes in an attempt to independently tune the structural and transport properties. In many cases immiscibility between the blocks induces microphase separation [24–26], producing ordered morphologies on the nanometer length scale [27]. The resulting copolymer retains the properties of each block, yielding a material with hard, insulating phases interspersed with soft, ionically conductive phases.

In studies utilizing block copolymers as SPE, the archetypal mechanical phase is made of a polymer with a high glass transition temperature (T_g) such as polystyrene (PS) [23,28–33]. For symmetric PS-PEO diblock copolymers [30–33] (SEO), the ionic conductivity σ has been shown to increase with PEO chain length and a plateau value is reached as the molecular weight of the PEO block exceeds 100 kg/mol. In contrast, σ of PEO homopolymers decreases with increasing molecular weight, reaching a plateau as the molecular weight of the PEO block exceeds 4 kg/mol [9]. Beyond PS-based block copolymers, a wide range of different amorphous polymers [34–39] has been considered for use as the structural block.

☆ Notes: The authors declare no competing financial interest.

* Correspondence to: G.W. Coates, Department of Chemistry and Chemical Biology, Baker Laboratory, Cornell University, Ithaca, NY 14853–1301, USA. Tel.: +1 607 255 5447.
** Correspondence to: N.P. Balsara, Department of Chemical Engineering, 201 Gilman Hall, University of California, Berkeley, CA 94720–1462, USA. Tel.: +1 510 642 8973.
E-mail addresses: gc39@cornell.edu (G.W. Coates), nbalsara@berkeley.edu (N.P. Balsara).

http://dx.doi.org/10.1016/j.ssi.2014.05.012
0167-2738/Published by Elsevier B.V.

In contrast to the extensive work described above featuring amorphous structural blocks, we are aware of only one publication wherein a semi-crystalline polymer was used as the structural block [40]. Many high volume commercial polymers, e.g. polyethylene and polypropylene, are semi-crystalline. Semi-crystalline polyolefin polymers have superior mechanical properties, are melt-processable, and exhibit excellent solvent resistance. The triblock copolymer studied therein was composed of polyethylene (PE) as the outer, structural blocks, and a copolymer of PEO and poly(propylene oxide) (P(EO-*co*-PO)) as the inner, ionically-conductive block. The ionic conductivity of this copolymer doped with LiTFSI was in the range of 2×10^{-4} S/cm at 90 °C. The molecular weight of the PE block was 0.7 kg/mol, which enabled dissolution of the electrolyte in organic solvent at room temperature. However the mechanical properties of SPEs in this molecular weight regime are well below the target molecular weight required to resist lithium dendrite growth [1,41]. It is obvious that higher molecular weight structural blocks are necessary to obtain robust SPEs with semi-crystalline structural blocks. We note in passing that the characteristics of the PE-P(EO-*co*-PO)-PE sample, obtained by coupling functionalized PE and bifunctional P(EO-*co*-PO) precursors, were not reported in Reference [40]. Polyolefins are in general chemically and electrochemically inert because they contain a saturated hydrocarbon backbone. Furthermore, semi-crystalline polyolefins, such as syndiotactic and isotactic polypropylene have improved solvent resistance in comparison to amorphous polymers.

Herein we report on the synthesis and characterization of a series of symmetric triblock copolymers composed of a central PEO block and a semi-crystalline syndiotactic polypropylene (sPP) as the outer blocks. The molecular weight of the sPP blocks ranges from 5 to 20 kg/mol. The polymers were obtained by coupling functionalized sPP chains and bifunctional PEO chains using click chemistry. Differential scanning calorimetry was used to characterize crystallinity, X-ray scattering was used to determine morphology, and AC impedance was used to determine ionic conductivity. The properties of these PEOP electrolytes were also compared with previously reported SEO block copolymer electrolytes.

2. Experimental

2.1. General synthesis methods

All manipulations of air- and/or water-sensitive compounds were carried out under dry nitrogen using a Braun UniLab drybox or standard Schlenk techniques. ^{1}H and ^{13}C NMR spectra were collected in deuterated solvents on a Varian INOVA 400 or Varian 500 (^{13}C, 125 MHz). The spectra were referenced internally to residual protio solvents (^{1}H) or to deuterio-solvent signals (^{13}C) and are reported relative to tetramethylsilane ($\delta = 0$ ppm). sPP samples were dissolved in $CDCl_3$ and NMR spectra were collected at 60 °C. Number-averaged molecular weights of the end-functionalized sPP and PEO samples were determined using end group analysis of quantitative ^{1}H NMR spectra and are given in Table 1 as $M_{n,sPP}$ and $M_{n,PEO}$.

2.1.1. Materials

Toluene was purified over columns of alumina and copper (Q5). Tetrahydrofuran for block copolymer synthesis was purified over alumina column and degassed by three freeze–pump–thaw cycles before use. Propylene (Airgas, research purity) was purified over columns of BASF catalyst R3-12, BASF catalyst R3-11, and 4 Å molecular sieves. Polymethylaluminoxane (PMAO-IP, 13 wt.% Al in toluene, Akzo Nobel) was dried in vacuo to remove residual trimethyl aluminum and used as a white solid powder. Sodium azide, PEO polymers (M_n: 3, 8, 16 and 38 kg/mol; polydispersity index PDI $= M_w/M_n =$ 1.02–1.12, where M_w is the weight-averaged molecular weight), para-toluenesulfonyl chloride, sodium hydride (60% dispersion in mineral oil), tripropargyl amine (98%), tetrakis(acetonitrile)copper(I) hexafluorophosphate (97%), 2,6-lutidine (>99%), borane-tetrahydrofuran complex (1.0 M solution in THF, stabilized with 0.005 M N-isopropyl-N-methyl-tert-butylamine), propargyl bromide solution (80 wt.% in toluene), and copper bromide were purchased from Sigma-Aldrich and used as received. Acetonitrile (HPLC grade) was obtained from Mallinckrodt Baker and used as received. Benzyl azide (94%) was purchased from Alfa-Aesar and used as received. $CDCl_3$ was purchased from Cambridge Isotope Laboratories (CIL) and used as received. Dry tetrahydrofuran (THF) for electrolyte preparation was obtained from Sigma-Aldrich and used as received in an argon-filled glove box. Dry LiTFSI was obtained from Novolyte under argon, brought into the glove box, and dried under vacuum in the glove box antechamber at 120 °C for three days prior to use.

Allyl-terminated sPP (PDI = 1.4–1.9) was prepared according to a previously reported procedure [42,43]. The extent of syndiotacticity of sPP samples was determined from ^{13}C NMR spectroscopy using the fraction of fully syndiotactic pentads [*rrrr*] and was found to be 0.80. Tris-(benzyltriazolylmethyl)amine (TBTA) ligand for alkyne-azide "click" chemistry was synthesized according to the literature procedure [44]. See Supporting information for the synthesis of the end functionalized polymers. End group analysis of a ^{1}H NMR spectrum obtained from the product of the sPP functionalization reaction determined the weight fraction of unfunctionalized sPP chains, $w_{sPP,h}$, which ranged from 0.17 to 0.43 and are given in Table 1.

Table 1
Polymer characteristics.

Polymer	$M_{n,sPP}$[a] (kg/mol)	PDI_{sPP}[b]	$M_{n,PEO}$[a] (kg/mol)	PDI_{PEO}[b]	ϕ_{PEO}	$w_{sPP,h}$[a]	ϕ_c
PEOP(4-3-4)	4.1	1.61	3.4	1.02	0.24	0.17	0.28
PEOP(4-8-4)	4.0	1.58	8.5	1.06	0.44	0.32	0.49
PEOP(4-16-4)	4.0	1.58	15.8	1.09	0.60	0.24	0.64
PEOP(5-16-5)	5.0	1.61	15.8	1.09	0.54	0.33	0.59
PEOP(10-38-10)	10.5	1.65	37.6	1.12	0.57	0.43	0.62

[a] Determined by ^{1}H NMR spectroscopy using end group analysis.
[b] Determined by gel permeation chromatography.

2.1.2. Synthesis of PEOP triblock copolymers

In the glovebox, a 100 mL Schlenk tube was charged with azido-terminated sPP (0.60 g, 0.070 mmol N_3 functional groups), dipropargyl-terminated PEO (0.36 g, 0.085 mmol functional propargyl groups), CuBr (3 mg, 0.02 mmol), and TBTA ligand (11 mg, 0.020 mmol). THF (7.1 mL) was added and the Schlenk tube was heated at 50 °C for 24 h. After the reaction had completed, the mixture was cooled to room temperature, and the polymer was precipitated in methanol. The resultant light green polymer was thoroughly washed with methanol to remove the copper catalyst and excess PEO. Insoluble polymer was isolated by vacuum filtration, washed with methanol, and dried in vacuo to constant weight (0.85 g, 94% yield). ^{1}H NMR (400 MHz, $CDCl_3$, 60 °C) δ 7.55 (s, 2H), 4.69 (s, 4H), 4.31 (t, $J = 7.4$ Hz, 4H), 3.64 (s, 1010H), and 1.70–0.58 (m, 2664H). ^{13}C NMR (126 MHz, $CDCl_3$, 60 °C) δ 70.85, 46.74, 27.74, and 19.97.

2.2. Electrolyte preparation

PEOP polymers were brought into an MBraun argon glove box for electrolyte preparation after drying in the glove box antechamber at 100 °C for one day. In the glove box, a mixture of PEOP polymer and dry LiTFSI was co-dissolved in THF. For all samples, the amount of LiTFSI added was predetermined to obtain a molar ratio *r* of lithium ions (Li^+) to ethylene oxide (EO) moieties equal to 0.063 ± 0.06. This salt concentration is in the vicinity of the optimum salt concentration for

SEO-based electrolytes [30]. The solution was stirred for several hours at 90 °C until complete dissolution was visually observed, and then the THF was allowed to evaporate to obtain a solid polymer–salt mixture. Subsequently, the electrolyte was dried further in the glove box antechamber under vacuum at 90 °C for at least 8 h prior to characterization.

For each electrolyte the volume fraction of the conducting phase, ϕ_c, is determined assuming that the LiTFSI is located in the PEO domain and that the volume change of mixing was negligible:

$$\phi_c(r) = \frac{V_{EO} + r \cdot V_{LiTFSI}}{V_{EO} + r \cdot V_{LiTFSI} + \frac{2 \cdot M_{n,sPP} \cdot M_{EO}}{M_P \cdot M_{n,PEO}} V_P} \quad (1)$$

where V_{EO}, V_{LiTFSI}, and V_P are the molar volumes of EO monomer units (41.56 cm^3/mol) [45], LiTFSI (141.9 cm^3/mol) [46], and propylene repeat units (105.99 cm^3/mol) [45], respectively, at a reference temperature of 140 °C. The values of ϕ_c for each polymer at the desired salt composition are given in Table 1.

2.3. Differential scanning calorimetry (DSC)

The thermal properties of polymers were studied via DSC experiments. Pure PEOP polymers and the related electrolytes were sealed in aluminum hermetic pans in an argon-filled glove box. DSC experiments were performed on a TA Instruments DSC Q200 instrument. All samples were subjected to the same thermal history: samples were heated from room temperature to 120 °C at 10 °C/min, after which two cooling/heating scans were run at 10 °C/min, between −40 °C and 120 °C. For each sample $T_{m,i}$ of the PEO and sPP microphases were determined at the maximum of each endothermic peak on the last cycle [47]. $T_{m,i}$ is the nominal melting temperature of the microphases, i = PEO or sPP. The integration of the area of each endothermic peak gives the enthalpy of melting, $\Delta H_{m,i}$, for each microphase i. The crystallinity, $X_{c,i}$, for the phase i is given by:

$$X_{c,i} = \frac{\Delta H_{m,i}}{w_i \cdot \Delta H^0_{m,i}} \quad (2)$$

where w_i is the weight fraction of phase i and $\Delta H^0_{m,i}$ is the enthalpy of melting of pure i. $\Delta H^0_{m,PEO}$ and $\Delta H^0_{m,sPP}$ values are 195.8 J/g and 206.7 J/g, respectively [48,49].

2.4. Small angle X-ray scattering (SAXS)

SAXS experiments were performed at beamline 7.3.3 at the Advanced Light Source (ALS) at Lawrence Berkeley National Laboratory and at beamline 1–4 at the Stanford Synchrotron Radiation Lightsource to determine the morphology and domain spacing of each block copolymer as well as the related electrolyte. SAXS samples were assembled in an argon-filled glove box by hot-pressing solid polymer samples with or without salt into approximately 150 μm thick spacers (Garolite G-10) at 90 °C. The samples were sealed in air-tight aluminum sample holders with Kapton windows, and annealed at 120 °C for several days prior to experiments. Samples were mounted in a custom-built sample stage with temperature (T) control. At each T examined, samples were annealed for a minimum of 20 min prior to data collection. SAXS data analysis was performed using the Nika program written for Igor Pro [50]. Silver behenate was used as a standard to calibrate beam center and sample-to-detector distance. The measured two-dimensional scattering data were azimuthally averaged to obtain intensity, I, as a function of the scattering vector magnitude, q. The relationship between q and the wavelength of the X-rays, λ, and the scattering angle, θ is given by:

$$q = \frac{4\pi}{\lambda} \sin\left(\frac{\theta}{2}\right). \quad (3)$$

The X-ray energy for SAXS experiments was approximately 10 keV in all cases, corresponding to $\lambda = 0.124\ nm^{-1}$. SAXS data from all the samples were obtained at room temperature and between 60 °C and 120 °C in increments of 20 °C. The location of the primary scattering peak at a scattering vector magnitude q^* enables determination of the domain spacing, d:

$$d = \frac{2\pi}{q^*}. \quad (4)$$

The ratio between q^* and higher order scattering peaks were used to determine the nanostructured morphology, e.g. integer multiples as indication of lamellar morphology ($q/q^* = 2, 3, 4$, etc.).

2.5. Resonant soft X-ray scattering (RSoXS)

RSoXS experiments were performed at beamline 11.0.1.2 at ALS to determine the domain size and morphology of high molecular weight samples for which q^* values could not be resolved by SAXS experiments ($q_{min,SAXS} \approx 0.1\ nm^{-1}$). RSoXS experiments could be performed over a range of incident X-ray energy values, which allows λ to be tuned and thus varies q_{min} according to Eq. (3) ($q_{min,RSoXS} \approx 0.03\ nm^{-1}$). Samples for RSoXS experiments were made by drop-casting in an argon-filled glove box to obtain thin samples which minimize X-ray absorption. Pure PEOP and LiTFSI-doped PEOP samples were made by dissolving the appropriate material in THF at a concentration of ~1 mg/mL solids at room temperature. Solutions were stirred overnight to ensure complete dissolution. The solutions were dropped onto silicon nitride substrates (Norcada) and dried overnight to obtain thin films on the order of 1–5 μm thick. The substrates consisted of a 200 μm thick silicon frame with dimensions 5 × 5 mm with a 100 nm thick silicon nitride top layer exposed in a 1.5 × 1.5 mm window. Samples were stored under argon until immediately before placement in the ultrahigh vacuum chamber used for RSoXS. Incident X-ray energies were tuned near the carbon K-edge to 280 eV. Samples were attached to a stage with carbon tape that was capable of heating samples to ~130 °C. Data were reduced and analyzed using a modified version of the Nika program for Igor Pro, and normalized by subtracting out a dark image to obtain $I(q)$ [51].

2.6. Symmetrical cell assembly and characterization

Inside an argon-filled glove box, the polymer electrolyte was hand-pressed at 90 °C into a 30 μm thick Kapton spacer with a 0.3 cm diameter hole that defines the active area S of the cell. Two stainless steel blocking electrodes were then placed on each side of the electrolyte-spacer assembly and pressed at 90 °C. At each step of the assembly the overall thickness was measured to monitor the electrolyte thickness, l. The average electrolyte thickness of the samples was 172 ± 18 μm. An aluminum tab was taped on each stainless steel electrode and the assembly was vacuum sealed in pouch material (Showa Denko).

The cells were mounted in to a custom heating stage and connected to a Bio-Logic VMP3. Impedance spectroscopy was performed using an excitation signal between 10 and 40 mV in a frequency range between 10^6 and 1 Hz. The T program consisted of an initial heating scan from room temperature to 120 °C in 10 °C steps, followed by cooling to room temperature, and then a second heating scan was carried out from 30 °C to 120 °C in 10 °C steps. Data was analyzed from the cooling scan and subsequent heating scan. For each T, the resistance of the electrolyte, R_{el}, was monitored as a function of time and the impedance

spectrum was recorded only when R_{el} became stable. The equilibrated value of R_{el} was extracted from the impedance spectra by fitting the profile with an equivalent electrical circuit consisting of a resistor and a constant phase element [52]. After the experiments, the cells were returned to the argon-filled glove box and disassembled to determine the final value of l. This l value was used to calculate σ according to Eq. (5):

$$\sigma(T) = \frac{l}{S \cdot R_{el}(T)} \tag{5}$$

at each T considered.

3. Results and discussion

3.1. PEOP synthesis and molecular characterization

PEOP block copolymers were synthesized using "click" coupling reaction of azide-terminated sPP (sPP-N_3) with the dipropargyl-terminated PEO (Scheme 1). The sPP–CH_2–CH_2–CH_2–N_3 was synthesized from allyl-terminated sPP (sPP–CH_2–CH═CH_2) in three consecutive steps in good yields [43,53,54]. The percent end group functionalization of sPP polymer was mainly dependent on hydroboration/oxidation conditions such as solvent, reaction time, and temperature. End group analysis of the sPP–N_3 polymers using ^{1}H NMR spectroscopy suggested that there is some proton-terminated sPP (sPP–CH_2–CH_2–CH_3) present in the sPP–N_3 polymer [53]. The unfunctionalized sPP resulting from this step is the primary source of sPP homopolymer in the final triblock material (denoted by $w_{sPP,h}$). The propargyl-terminated PEO was synthesized from commercially available PEO in one step using the Williamson ether reaction of the deprotonated PEO with the propargyl bromide [53]. Conversion of the hydroxyl to the propargyl-terminated PEO proceeded with high efficiency (>95%) according to the end group analysis using ^{1}H NMR spectroscopy.

Synthetic methodologies to obtain amphiphilic block copolymers, which are comprised of PEO as an ion-conducting block and a semi-crystalline polymer as a structural block, remain limited [55,56]. Recently Zhu and coworkers reported azide–alkyne "click" coupling reaction to synthesize sPP-*b*-PEO diblock copolymers [56]. We used similar "click" chemistry methods to obtain amphiphilic PEOP triblock copolymers in this work. A coupling reaction of sPP–N_3 was performed with dipropargyl-terminated PEO using Cu(I) as the catalyst and TBTA as the ligand to obtain PEOP triblock copolymers [44]. The PEOP triblock copolymers synthesized for this study are listed in Table 1. Successful coupling of the functionalized sPP block and PEO block was confirmed by ^{1}H NMR spectroscopy (Fig. S1). The characteristic peak of triazole moiety at δ 7.55 ppm confirmed the "click" reaction and formation of PEOP triblock copolymer. Each of the PEOP triblock copolymer samples contained a portion of unfunctionalized sPP homopolymer that was not able to react with functionalized PEO homopolymer and could not be removed from the triblock copolymer (see Table 1). The presence of this sPP homopolymer might influence the mechanical properties and ionic conductivity of the PEOP electrolytes. Nonetheless, we used these PEOP triblock copolymers without further purification for the thermal, morphological, and electrochemical studies described subsequently.

High temperature gel permeation chromatography (GPC) analyses of PEOP triblock copolymers do not reflect a significant increase in molecular weight (Fig. S2). Presumably, this is due to an insignificant change in hydrodynamic radii of the PEOP polymer and the presence of sPP homopolymer. Direct proof of the coupling reaction is thus contained in the ^{1}H NMR spectroscopy results only.

3.2. PEOP thermal properties

All of the neat PEOP triblock copolymers exhibited two melting transitions in the vicinity of the melting points of sPP and PEO homopolymers. This indicates the existence of strongly segregated microphases. The results of these experiments are summarized in Fig. 1a, where T_m of each block is shown as a function of total triblock molecular weight (M_n). The measured $T_{m,sPP}$ for high-M_n sPP is significantly reduced compared with previously reported values for homopolymer sPP and sPP-containing block copolymers, albeit for polymers which generally possess much larger M_n than that considered here. The values for $T_{m,sPP}$ represent the maximum value for the endothermic peak observed on heating the sample. Within experimental error, $T_{m,sPP}$ was found to be independent of M_n, with an average value of 105 ± 5 °C. Thermal transitions are also affected by the degree of syndiotacticity. De Rosa and coworkers synthesized sPP homopolymers of varying syndiotacticities and observed a reduction in $T_{m,sPP}$ with decreasing syndiotacticity [57]. In the sPP-containing block copolymers studied here, the tacticity of sPP is approximately 80% corresponding to a homopolymer melting temperature of 116 °C, based on an extrapolated linear relationship between $T_{m,sPP}$ and % [*rrrr*] [58]. Thus the values of $T_{m,sPP}$ reported here seem reasonable. It is possible that the presence of covalently-bonded PEO blocks interferes with the sPP crystallization process, leading to a further reduction of $T_{m,sPP}$. In contrast to PP crystallization, $T_{m,PEO}$ is observed to increase monotonically with increasing M_n, from 38 to 63 °C ($M_{n,PEO}$ increases by approximately one order of magnitude, see Table 1).

The dependence of percent crystallinity, $X_{c,i}$, in each microphase, determined by DSC, is shown in Fig. 1b. Both $X_{c,sPP}$ and $X_{c,PEO}$ are independent of M_n; $X_{c,sPP} = 16 \pm 3\%$ while $X_{c,PEO} = 41 \pm 4\%$.

DSC experiments were carried out for samples doped with LiTFSI to establish changes in the PEOP physical properties when utilized as an electrolyte. Fig. 2a shows the plot of T_m of each block as a function of M_n. The samples were prepared at a salt concentration of $r = 0.063 \pm 0.006$. This corresponds to a weight fraction $w_{Li/EO}$ of 0.29 ± 0.02 of

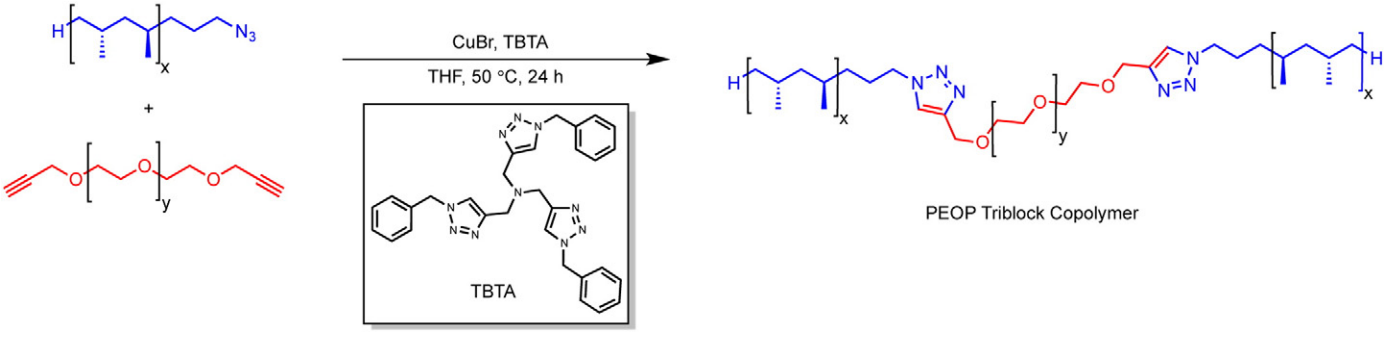

Scheme 1. Synthesis of syndiotactic polypropylene-*b*-poly(ethylene oxide)-*b*-syndiotactic polypropylene (PEOP) triblock copolymers.

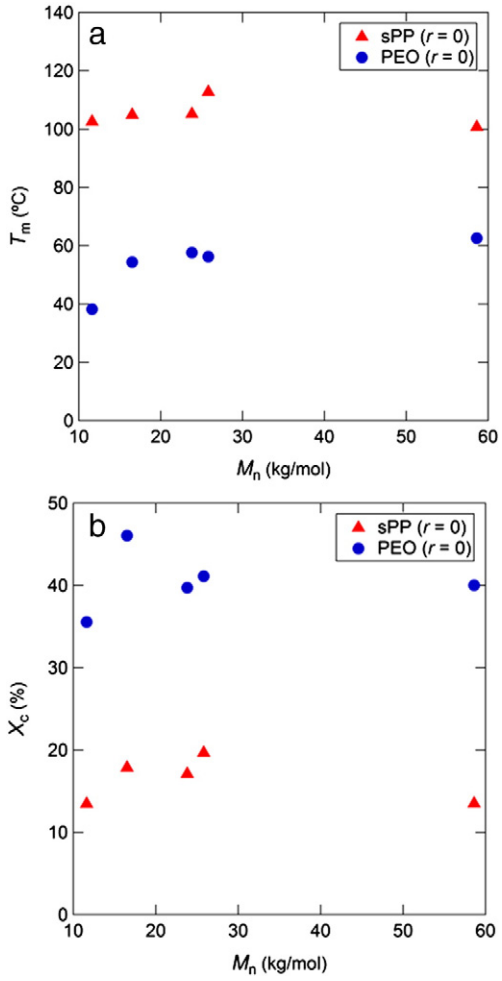

Fig. 1. Melting temperature (a) and percent crystallinity (b) of sPP and PEO blocks in neat PEOP triblock copolymer as a function of total molecular weight.

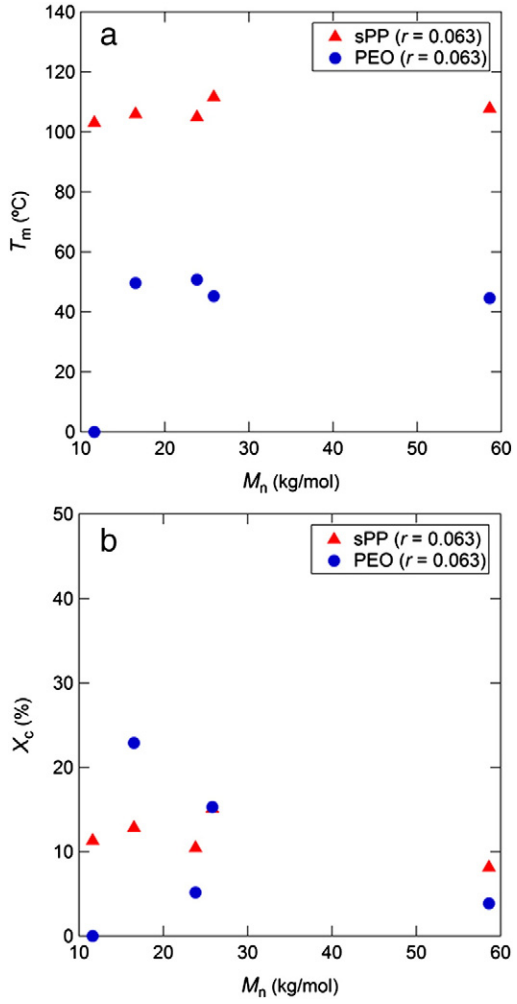

Fig. 2. Melting temperature (a) and crystallinity (b) of sPP and PEO blocks in LiTFSI-doped PEOP triblock copolymer as a function of total molecular weight.

LiTFSI in the PEO domains, assuming that LiTFSI is completely solubilized by the PEO chains [33,59]. In the salt-containing PEOP samples, there is no dependence of $T_{m,sPP}$ on M_n, and the samples have an average value of 107 ± 3 °C which is within experimental error of $T_{m,sPP}$ of the neat triblock copolymers (105 ± 5 °C). It is evident that the addition of LiTFSI has no effect on the crystalline nature of sPP, supporting the hypothesis that the salt is fully segregated to PEO domains. The lowest-M_n copolymer, PEOP(4-3-4), has no measurable crystallinity when doped with LiTFSI. Signatures of PEO crystallization remained absent when the temperature scan rate was decreased to 5 °C/min, suggesting that the presence of salt completely suppresses crystallization of PEOP(4-3-4). Aside from PEOP(4-3-4), the other four samples studied exhibited DSC peaks consistent with PEO crystallization even in the presence of LiTFSI but with a reduction in $T_{m,PEO}$ to a value that was roughly independent of M_n equal to 48 ± 3 °C (Fig. 2a). This result agrees with the findings described by Yuan et al. [46], for SEO electrolytes, where low M_n electrolytes ($M_{n,PEO}$ < 8 kg/mol) show no observable crystallinity, while in the high-M_n case $T_{m,PEO}$ was in reasonable agreement with $T_{m,PEO}$ observed here for PEOP.

The dependence of $X_{c,i}$ in each microphase of the salt containing samples, determined by DSC, is shown in Fig. 2b. The addition of LiTFSI results in a slight decrease $X_{c,sPP}$ from 16 ± 3% to 12 ± 3%. In contrast, the addition of LiTFSI has a significant impact on PEO crystallinity. The average value of $X_{c,PEO}$ for the samples containing a non-zero crystalline fraction with added salt was equal to 12 ± 9% compared to 41 ± 4% for the salt-free PEOP polymer. This strong effect of LiTFSI on PEO crystallinity is expected. PEO solvates lithium ions via coordination with the ether oxygen. This coordination interferes with crystallization [12].

3.3. PEOP morphological characterization

We performed SAXS experiments on the neat PEOP as well as LiTFSI-doped material to study microphase separation. Fig. 3 shows the SAXS profiles for neat and salt-doped PEOP. The measurements were done at 120 °C, well above T_m for the PEO and sPP microphase. The morphology of PEOP(4-3-4) in both neat and salt doped states is clearly resolved by SAXS. In the neat state, the higher order peaks are located at q values which have ratio $q/q^* = 3^{1/2}$, $7^{1/2}$, and $9^{1/2}$, indicative of the hexagonally-packed cylindrical morphology as expected for a block copolymer with $\phi_{PEO} = 0.24$ (Table 1). In the salty state, the higher order peaks are located at ratio $q/q^* = 2$, 3, 4, and 5 indicative of a lamellar geometry. The change in the morphology of PEOP(4-3-4) electrolyte from cylinders to lamellae is surprising because the addition of LiTFSI increases the volume fraction of the conducting phase from 0.24 to 0.27. Neat PEOP(4-8-4), with a larger $\phi_{PEO} = 0.44$, displayed higher order peaks at $q/q^* = 2$, 4, and 5, indicating a lamellar morphology. The addition of salt does not alter the dominant morphology of PEOP(4-8-4); q/q^* of the higher peaks with and without salt are similar. The presence of satellite peaks of the SAXS profile of salt containing PEOP(4-8-4) suggests the presence of a small amount of a second

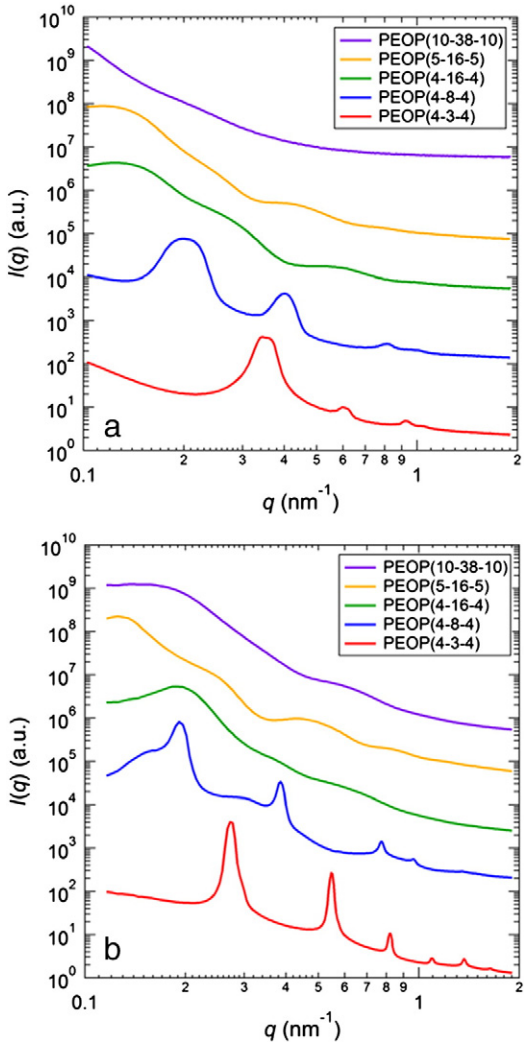

Fig. 3. SAXS profiles for PEOP samples in the absence (a) and presence (b) of LiTFSI, at 120 °C.

microphase. The presence of coexisting microphases in salt-containing block copolymers has been established in previous studies [60–62]. Both neat and salt containing PEOP(4-16-4) and PEOP(5-16-5) samples show primary SAXS peak close to the resolution limit of the SAXS instrument. The primary peak of neat PEOP(10-38-10) is outside the limit of the SAXS instrument while that of the salt-containing PEOP(10-38-10) is within the limit of the SAXS instrument. The absence of well-defined higher ordered peaks in PEOP(4-16-4), PEOP(5-16-5) and PEOP(10-38-10) precludes the determination of the morphology of these systems. In the presence of salt, ϕ_c of these samples varies between 0.59 and 0.64. In the analysis below, we assume that these systems have a lamellar morphology. The SAXS peaks in salt-containing PEOP(4-3-4) and PEOP(4-8-4) are much less sharp than the peaks in the neat case. This suggests the presence of a range of domain size, which is not seen in salt-containing SEO block copolymers.

We used RSoXS to complement the SAXS measurements described above. In Fig. 4 we show the RSoXS profile obtained for neat PEOP(10-38-10). A primary peak at $q^* = 0.0726\ \mathrm{nm}^{-1}$ indicates a domain spacing of 86.5 nm. To ensure the robustness of the RSoXS approach, we also examined PEOP(4-3-4) in the absence and presence of salt. The SAXS and RSoXS data from these samples are in qualitative agreement with each other but not in quantitative agreement. For example, for neat PEOP(4-3-4) $d_{\mathrm{RSoXS}} = 16.4$ nm while $d_{\mathrm{SAXS}} = 18.0$ nm. We attribute this difference to multiple scattering in the RSoXS experiment.

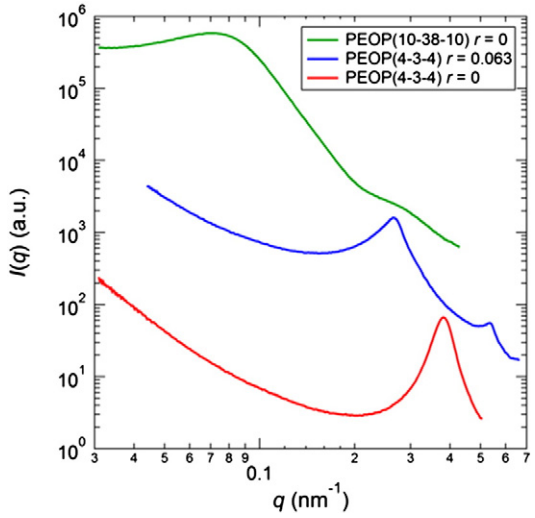

Fig. 4. RSoXS profiles for PEOP(4-3-4) in the absence and presence of LiTFSI and neat PEOP(10-38-10), at 120 °C.

The dependence of d on M_n obtained in our samples by a combination of SAXS and RSoXS is shown in Fig. 5. The data are roughly consistent with the expected $d \sim M_n^{0.67}$ scaling law for strongly segregated block copolymers.

3.4. PEOP ionic conductivity

The ionic conductivity σ of the PEOP electrolytes doped with LiTFSI is plotted as a function of $1000/T$ in Fig. 6. Before discussing electrolyte conductivities, we discuss data obtained for PEOP(4-16-4) in the absence of LiTFSI (i.e., $r = 0$), also shown in Fig. 6. In the absence of impurities the ionic conductivity of this sample should be equal to zero. In contrast we find σ values ranging from 3×10^{-6} to 1×10^{-5} S/cm at $T > 50$ °C (above $T_{m,PEO}$). Below 50 °C (i.e. $T < T_{m,PEO}$), σ decreases abruptly to 1×10^{-7} S/cm. The conductivity of the PEOP samples with salt is significantly higher than that of neat PEOP(4-16-4); typically the electrolyte conductivity is a factor of 10 to 100 larger than that of neat PEOP(4-16-4). One may regard the measured conductivity of neat PEOP(4-16-4) as a measure of

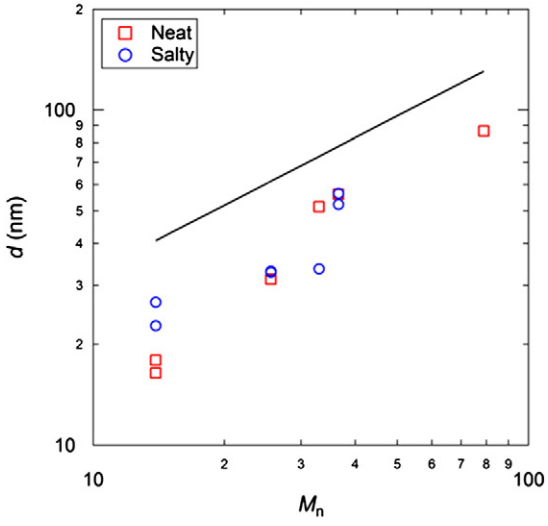

Fig. 5. Domain spacing of neat (red squares) and salty (blue circles) PEOP block copolymers obtained from SAXS and RSoXS measurements as a function of molecular weight. The expected scaling law for block copolymers $d \sim M_n^{0.67}$ is represented by the solid black line.

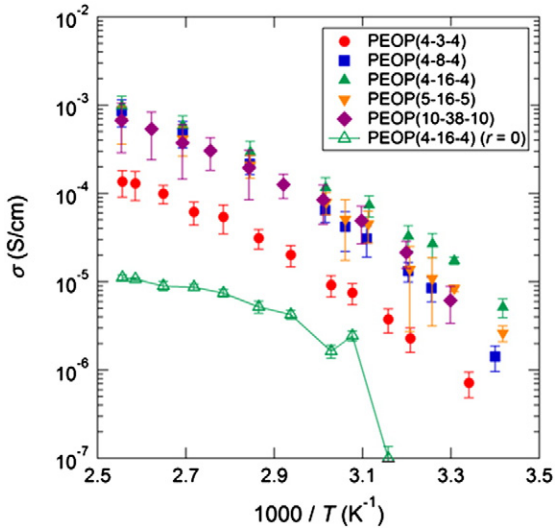

Fig. 6. Ionic conductivity of LiTFSI-doped PEOP block copolymers and neat PEOP(4-16-4) as a function of 1000/*T*.

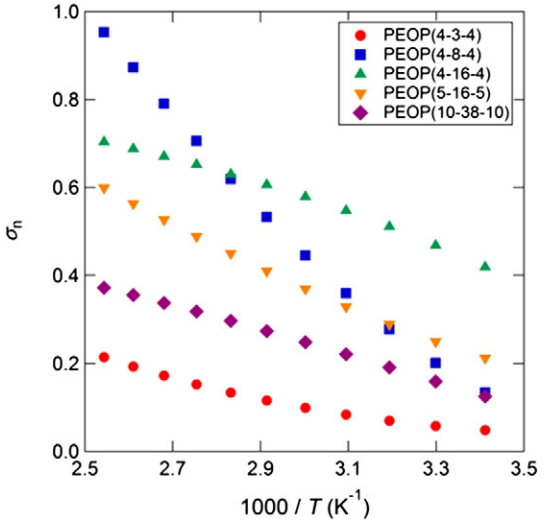

Fig. 7. Normalized conductivity, as a function of 1000/*T* for LiTFSI-doped PEOP.

the "background" conductivity due to the presence of impurities. We ignore this effect in the discussion below.

It is interesting to note that the temperature dependence of the conductivity of all electrolytes is smooth over the measured temperature window. In other words, neither $T_{m,sPP}$ nor $T_{m,PEO}$ of the salt-containing electrolytes has a noticeable effect on the conductivity.

The ionic conductivity values of the PEOP electrolytes are affected by both ϕ_c and M_n. In order to separate these two effects, we define normalized conductivity σ_n [30]

$$\sigma_n(r,T) = \frac{\sigma(r,T)}{f\cdot\phi_c\cdot\sigma_{PEO}(r,T)} \tag{7}$$

where f is a morphology factor that accounts for the geometry of the conducting phase, and σ_{PEO} is the conductivity of PEO homopolymer (M_n = 4 kg/mol) doped with LiTFSI at the salt concentration and temperature of interest [12]. Based on the considerations given above we assume a lamellar morphology for all samples, and $f = 2/3$ [32].

To facilitate comparison of conductivity at a fixed temperature, we fit the measured conductivity of the PEOP samples to the empirical Vogel–Tamman–Fulcher (VTF), shown in Eq. (8) [63–65]:

$$\sigma(T) = \frac{\sigma_0}{\sqrt{T}}\cdot\exp\left(\frac{-B}{R\cdot(T-T_0)}\right). \tag{8}$$

Here R is the gas constant and T_0 is the ideal glass transition temperature, which is fixed at a value of −90 °C [46]. The two fitting parameters are the pre-exponential factor σ_0, which is related to the concentration of free charges, and B, which is related to the activation energy These parameters were adjusted to fit the data ($\chi^2 > 0.99$). The fitted values of σ_0 and B thus obtained are given in Table 2. Also given in Table 2 are fitted parameters for the PEO homopolymer used to determine σ_{PEO}. For the PEOP electrolytes, we found that the values for B are very similar for each composition with an average of 11.4 ± 0.9 kJ/mol while σ_0 is higher for the most conductive electrolytes. This enables the calculation of σ_n of all our samples at selected temperatures, and the results of this calculation are shown in Fig. 7. The slopes of σ_n vs. 1000/*T* for each of our samples, with the exception of PEOP(4-8-4), are similar. At *T* greater than 100 °C, PEOP(4-8-4) has the highest σ_n of all polymers studied, and approaches a value of 1.0 at 120 °C.

Table 2
VTF parameters.

Polymer	σ_0 (S/cm · K$^{1/2}$)	B (kJ/mol)
PEO(4)	9.3	8.4
PEOP(4-3-4)	2.9	11.9
PEOP(4-8-4)	34.1	12.8
PEOP(4-16-4)	9.3	10.4
PEOP(5-16-5)	8.4	10.9
PEOP(10-38-10)	9.0	11.1

Fig. 8 shows the dependence of σ_n on M_n at 90 °C for the PEOP and SEO [46] electrolytes. It is striking that σ_n exhibits a peak at M_n values between 15 and 25 kg/mol. As discussed above the main difference between the PEOP electrolytes is the value of the pre-exponential factor, σ_0. It is perhaps somewhat surprising that changes in the structural block with molecular weight affect σ_0, a parameter that is believed to reflect the concentration of free ions in the conducting block. The data in Fig. 8 is very different from previous data obtained from block copolymer electrolyte with amorphous structural blocks (e.g. SEO). In SEO copolymers σ_n increases monotonically as M_n increases from 10 kg/mol approaching a plateau in the high-M_n limit. The results for the SEO electrolytes suggest that the connectivity of the conducting lamellae phase is unaffected by increasing the molecular weight of the

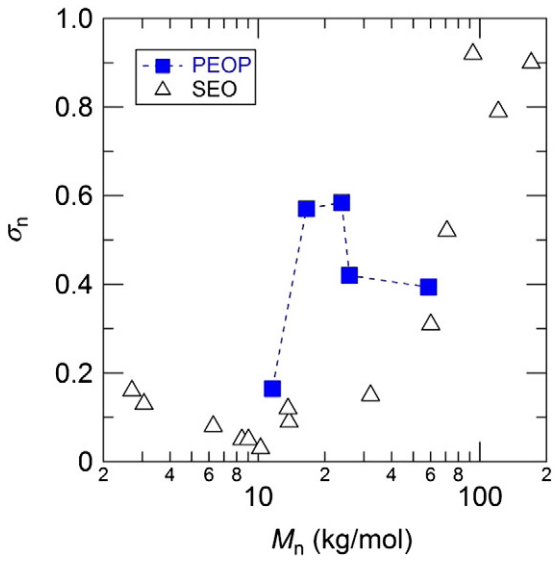

Fig. 8. Dependence of σ_n on M_n for PEOP (filled symbols) and SEO (hollow symbols; reference [46]) electrolytes at 90 °C.

amorphous structural block. The PEOP results presented in Fig. 8 suggest that high molecular weight semi-crystalline structural blocks affect the connectivity of the conducting lamellae. The extent to which our results are impacted by the unfunctionalized sPP homopolymer is unclear at this point.

4. Conclusions

We have synthesized and characterized the self-assembly of syndiotactic polypropylene-block-poly(ethylene oxide)-block-syndiotactic polypropylene triblock copolymers, and established their unusual behavior as solid polymer electrolytes. Due to the synthetic challenge to produce such copolymer, the samples were not ideal and the fraction of uncoupled syndiotactic polypropylene chains has been quantified. Using DSC and scattering experiments, the thermal and structural properties of the polymers were analyzed, and the effect of doping with lithium bis(trifluoromethane)sulfonimide salt was determined. The normalized ionic conductivity showed a maximum in the intermediate molecular weight range, at about 20 kg/mol. Such behavior is unusual when compared to solid polymer electrolyte comprising a glassy mechanical reinforced block. This is the most complete study to date of a block copolymer electrolytes with semi-crystalline blocks, and it may enable the design of improved solid polymer electrolytes.

Acknowledgments

The authors thank Daniel Hallinan and Alexander Teran for their helpful discussions. This work was supported by the Assistant Secretary for Energy Efficiency and Renewable Energy, Office of Vehicle Technologies of the US Department of Energy under Contract No. DE-AC02-05CH11231 under the Batteries for Advanced Transportation Technologies (BATT) Program. Part of this work was supported by the Energy Materials Center at Cornell (EMC2), an Energy Frontier Research Center funded by the US Department of Energy, Office of Science, Office of Basic Energy Sciences under Award Number DE-SC0001086. Portions of this work were carried out at the Advanced Light Source at Lawrence Berkeley National Laboratory, which is supported by the Director, Office of Science, Office of Basic Energy Sciences, of the US Department of Energy under Contract No. DE-AC02-05CH11231, and at the Stanford Synchrotron Radiation Laboratory, a national user facility operated Stanford University on behalf of the US Department of Energy, Office of Basic Energy Sciences. We acknowledge Alex Hexemer, Cheng Wang, Eric Schaible, Anthony Young, and John Pople for their help with SAXS.

Appendix A. Supplementary data

Supplementary data to this article can be found online at http://dx.doi.org/10.1016/j.ssi.2014.05.012.

References

[1] C. Monroe, J. Newman, J. Electrochem. Soc. 152 (2005) A396.
[2] M. Armand, Solid State Ionics 69 (1994) 309.
[3] R. Bouchet, S. Maria, R. Meziane, A. Aboulaich, L. Lienafa, J.-P. Bonnet, T.N.T. Phan, D. Bertin, D. Gigmes, D. Devaux, R. Denoyel, M. Armand, Nat. Mater. 12 (2013) 452.
[4] D.T. Hallinan, N.P. Balsara, Annu. Rev. Mater. Res. 43 (2013) 503.
[5] D.E. Fenton, J.M. Parker, P.V. Wright, Polymer 14 (1973) 589.
[6] M. Armand, J.M. Chabagno, M.J. Duclot, in: P. Vashishta, J.N. Mundy, G.K. Shenoy (Eds.), Fast Ion Transport in Solids Electrodes and Electrolytes, Amsterdam, North-Holland, 1979, pp. 131–136.
[7] M. Armand, Solid State Ionics 9–10 (1983) 745.
[8] D. Baril, C. Michot, M. Armand, Solid State Ionics 94 (1997) 35.
[9] J. Shi, C.A. Vincent, Solid State Ionics 60 (1993) 11.
[10] D. Diddens, A. Heuer, O. Borodin, Macromolecules 43 (2010) 2028.
[11] A. Vallée, S. Besner, J. Prudhomme, Electrochim. Acta 37 (1992) 1579.
[12] S. Lascaud, M. Perrier, A. Vallée, S. Besner, J. Prudhomme, M. Armand, Macromolecules 27 (1994) 7469.
[13] M. Dollé, L. Sannier, B. Beaudoin, M. Trentin, J.-M. Tarascon, Electrochem. Solid-State Lett. 5 (2002) A286.
[14] M. Rosso, C. Brissot, A. Teyssot, M. Dollé, L. Sannier, J.-M. Tarascon, R. Bouchet, S. Lascaud, Electrochim. Acta 51 (2006) 5334.
[15] W.H. Hou, C.Y. Chen, C.C. Wang, Y.H. Huang, Electrochim. Acta 48 (2003) 679.
[16] Y.H. Liang, C.C. Wang, C.Y. Chen, Eur. Polym. J. 44 (2008) 2376.
[17] J.F. Snyder, R.H. Carter, E.D. Wetzel, Chem. Mater. 19 (2007) 3793.
[18] K. Hayamizu, Y. Aihara, W.S. Price, J. Chem. Phys. 113 (2000) 4785.
[19] D.R. Sadoway, J. Power Sources 129 (2004) 1.
[20] P.E. Trapa, M.H. Acar, D.R. Sadoway, A.M. Mayes, J. Electrochem. Soc. 152 (2005) A2281.
[21] P.E. Trapa, Y.Y. Won, S.C. Mui, E.A. Olivetti, B.Y. Huang, D.R. Sadoway, A.M. Mayes, S. Dallek, J. Electrochem. Soc. 152 (2005) A1.
[22] Q. Hu, S. Osswald, R. Daniel, Y. Zhu, S. Wesel, L. Ortiz, D.R. Sadoway, J. Power Sources 196 (2011) 5604.
[23] T. Niitani, M. Shimada, K. Kawamura, K. Kanamura, J. Power Sources 146 (2005) 386.
[24] L. Leibler, Macromolecules 13 (1980) 1602.
[25] M.W. Matsen, R.B. Thompson, J. Chem. Phys. 111 (1999) 7139.
[26] M.W. Matsen, J. Chem. Phys. 113 (2000) 5539.
[27] V. Abetz, T. Goldacker, Macromol. Rapid Commun. 21 (2000) 16.
[28] T. Niitani, M. Shimada, K. Kawamura, K. Dokko, Y.H. Rho, K. Kanamura, Electrochem. Solid-State Lett. 8 (2005) A385.
[29] T. Niitani, M. Amaike, H. Nakano, K. Dokko, K. Kanamura, J. Electrochem. Soc. 156 (2009) A577.
[30] M. Singh, O. Odusanya, G.M. Wilmes, H.B. Eitouni, E.D. Gomez, A.J. Patel, V.L. Chen, M.J. Park, P. Fragouli, H. Iatrou, N. Hadjichristidis, D. Cookson, N.P. Balsara, Macromolecules 40 (2007) 4578.
[31] S.A. Mullin, G.M. Stone, A. Panday, N.P. Balsara, J. Electrochem. Soc. 158 (2011) A619.
[32] A. Panday, S. Mullin, E.D. Gomez, N. Wanakule, V.L. Chen, A. Hexemer, J. Pople, N.P. Balsara, Macromolecules 42 (2009) 4632.
[33] E.D. Gomez, A. Panday, E.H. Feng, V. Chen, G.M. Stone, A.M. Minor, C. Kisielowski, K. H. Downing, O. Borodin, G.D. Smith, N.P. Balsara, Nano Lett. 9 (2009) 1212.
[34] P. Lobitz, H. Fullbier, A. Reiche, J.C. Illner, H. Reuter, S. Horing, Solid State Ionics 58 (1992) 41.
[35] F. Alloin, J.-Y. Sanchez, M. Armand, Electrochim. Acta 37 (1992) 1729.
[36] J. Saunier, F. Alloin, J.-Y. Sanchez, Electrochim. Acta 45 (2000) 1255.
[37] K. Jankova, P. Jannasch, S. Hvilsted, J. Mater. Chem. 14 (2004) 2902.
[38] L.L. Ionescu-Vasii, Y. Abu-Lebdeh, M. Armand, Solid State Ionics 176 (2005) 2769.
[39] J. Huang, Z.-Z. Tong, B. Zhou, J.-T. Xu, Z.-Q. Fan, Polymer 54 (2013) 3098.
[40] P. Jannasch, Chem. Mater. 14 (2002) 2718.
[41] G.M. Stone, S.A. Mullin, A.A. Teran, D.T. Hallinan, A.M. Minor, A. Hexemer, N.P. Balsara, J. Electrochem. Soc. 159 (2012) A222.
[42] A.E. Cherian, E.B. Lobkovsky, G.W. Coates, Macromolecules 38 (2005) 6259.
[43] A.M. Anderson-Wile, G.W. Coates, F. Auriemma, C. De Rosa, A. Silvestre, Macromolecules 45 (2012) 7863.
[44] T.R. Chan, R. Hilgraf, K.B. Sharpless, V.V. Fokin, Org. Lett. 6 (2004) 2853.
[45] N.P. Balsara, H.B. Eitouni, in: J.E. Mark (Ed.), Physical Properties of Polymers Handbook, Second Edition, Springer, New York, 2007, pp. 339–356.
[46] R. Yuan, A.A. Teran, I. Gurevitch, S.A. Mullin, N.S. Wanakule, N.P. Balsara, Macromolecules 46 (2013) 914.
[47] M. Marzantowicz, F. Krok, J.R. Dygas, Z. Florjanczyk, E. Zygadlo-Monikowska, Solid State Ionics 179 (2008) 1670.
[48] C.P. Buckley, A.J. Kovacs, Colloid Polym. Sci. 254 (1976) 695.
[49] P. Supaphol, J. Appl. Polym. Sci. 79 (2001) 1603.
[50] J. Ilavsky, J. Appl. Crystallogr. 45 (2012) 324.
[51] E. Gann, A.T. Young, B.A. Collins, H. Yan, J. Nasiatka, H.A. Padmore, H. Ade, A. Hexemer, C. Wang, Rev. Sci. Instrum. 83 (2012) 045110.
[52] D. Devaux, R. Bouchet, D. Glé, R. Denoyel, Solid State Ionics 227 (2012) 119.
[53] See Supporting Information for Details.
[54] A.M. Anderson, Development of Functionalized Polymers Using Bis(phenoxyimine) titanium and Alpha-diimine Nickel(II) Catalysts for the Production of New Polyolefin Architectures, Chemistry and Chemical Biology, , Cornell University, Ithaca, 2010.
[55] M.A. Hillmyer, F.S. Bates, Macromolecules 29 (1996) 6994.
[56] R. Liu, Z.-Y. Li, B.-Y. Mai, Q. Wu, G.-D. Liang, H.-Y. Gao, F.-M. Zhu, J. Polym. Res. 20 (2013) 2.
[57] O. Ruiz de Ballesteros, F. Auriemma, C. De Rosa, Macromolecules 40 (2007) 611.
[58] C. De Rosa, O. Ruiz de Ballesteros, F. Auriemma, Macromolecules 37 (2004) 7724.
[59] F.I. Allen, M. Watanabe, Z. Lee, N.P. Balsara, A.M. Minor, Ultramicroscopy 111 (2011) 239.
[60] N.S. Wanakule, A. Panday, S.A. Mullin, E. Gann, A. Hexemer, N.P. Balsara, Macromolecules 42 (2009) 5642.
[61] A.A. Teran, N.P. Balsara, J. Phys. Chem. B 118 (2014) 4.
[62] I. Nakamura, N.P. Balsara, Z.G. Wang, ACS Macro Lett. 2 (2013) 478.
[63] H. Vogel, Phys. Z. 22 (1921) 645.
[64] V.G. Tamman, W. Hesse, Z. Anorg. Allg. Chem. 156 (1926) 245.
[65] G.S. Fulcher, J. Am. Ceram. Soc. 8 (1925) 339.